April 1987 LRP 321/87

LOW FREQUENCY RF HEATING ON TCA USING ALFVEN WAVES

K. Appert, G. Besson, G.G. Borg, B.P. Duval,
A.A. Howling, B. Joye, J.B. Lister, J.-M. Moret
F. Ryter, J. Vaclavik and H. Weisen

Invited Paper presented at the

1987 International Conference on Plasma Physics
Kiev, USSR - April 6-12, 1987

by

J.B. Lister

LOW FREQUENCY RF HEATING ON TCA USING ALFVEN WAVES

K. Appert, G. Besson, G.G. Borg, B.P. Duval, A.A. Howling,
B. Joye, J.B. Lister, J.-M. Moret, F. Ryter, J. Vaclavik and H. Weisen

Centre de Recherches en Physique des Plasmas
Association Euratom - Confédération Suisse
Ecole Polytechnique Fédérale de Lausanne
21, Av. des Bains, CH-1007 Lausanne/Switzerland

presented by J.B. Lister

ABSTRACT

We present some new results on the excitation of Alfvén Waves in the TCA tokamak, including properties of the external rf wavefield which are indicative of the importance of kinetic effects, and observations of the internal fluctuations for travelling waves. A parametric analysis of the density rise is used to quantify its evolution when the rf power is applied and when the excited spectrum changes. Changes in the excited spectrum also provoke variations in the plasma equilibrium, in the column resistance and in the MHD activity. The variations in $\beta_\perp$ and $\beta+li/2$ are presented together with preliminary results from rf power modulation experiments.

1. INTRODUCTION

The TCA Tokamak has major and minor radii R_o,a = 0.61 and 0.18 m, toroidal magnetic field B_ϕ up to 1.51 T, and plasma currents up to 135 kA in the present work. It has a circular plasma cross-section, and is fully equipped to study rf plasma heating using Alfvén Waves. Operation is in both hydrogen and deuterium, with carbon limiters.

The Shear Alfvén Wave resonance criterion is satisfied when $\omega = k_\parallel V_A$, where V_A is the local value of the Alfvén speed. This condition can be re-expressed in an equivalent periodic cylindrical geometry as

$$\omega^2(r) = \left(\frac{1}{R_o}\right)^2 \left(n + \frac{m}{q(r)}\right)^2 \left(\frac{B_o^2}{\mu_o \rho(r)}\right)\left(1 - \frac{\omega^2}{\omega_{ci}^2}\right) \qquad (1)$$

in which n,m are the toroidal and poloidal mode numbers respectively, q(r) and $\rho(r)$ are the local values of the safety factor and mass density, and ω_{ci} is the ion-cyclotron frequency. Shear Alfvén Waves in cold toroidal plasmas have been studied by APPERT et al. (1986) who showed primarily that the principles

of Shear Alfvén Wave excitation are maintained when going from a 1-D to a 2-D geometry; specifically, the wave excitation remains localised on magnetic surfaces. This fact allows us to use many of the results from 1-D calculations as being generalisable to a toroidal plasma.

From Equation (1), the resonance frequency near the axis lies in the MHz range, for low values of the toroidal mode number n. This does not vary particularly from one tokamak to another, due to the fact that the mass density will be bounded by the normal tokamak density operational limit: $\bar{n}_e < N_M \times B_\phi/R_O$, where N_M is the Murakami parameter. The range of frequencies for the resonance condition will then typically vary as $\omega \sim (B_\phi/R_O\langle A\rangle)^{1/2}$ where $\langle A\rangle$ is the average ion mass per electron. The factor $(B_\phi/R_O)^{1/2}$ ranges from, for example, 1.6 for a high current density tokamak such as TCA, to ~1.0 for a large tokamak such as NET. The operational frequency of TCA, 2.5 MHz for the results to be presented in this paper, is therefore typical of low-n Alfvén Wave Heating in general. The driving frequency will always be less than ω_{ci}.

The radial dependences of $\rho(r)$ and $q(r)$ for a typical tokamak plasma lead to the standard resonance curves of minor radius versus line-integrated electron density, shown in Fig. 1(a) for the case of n = 2. The positions and numbers of excited resonance surfaces depend on the plasma density. An increase in plasma density during a discharge will therefore correspond, in an experiment at fixed frequency, to a change in the positions and mode numbers of the resonance layers, which we will refer to as a change in the "excited spectrum".

To excite the Shear Alfvén Wave in the interior of the plasma, use is made of the strong external coupling at low frequency to the non-axisymmetric fast wave, often referred to as the surface wave. The deep radial penetration of this wave allows it to couple to, and therefore transfer its energy to, the Shear Alfvén Wave. To maximise the coupling from an external antenna, we must drive an external oscillating toroidal field ($\tilde{b}_\phi$) which causes a large oscillating pressure modulation in the presence of the large static toroidal magnetic field ($\tilde{p} \sim \tilde{b}_\phi B_\phi/\mu_O$), generally at least an order of magnitude greater than the poloidal magnetic field. The oscillating field is generated by antenna currents in the poloidal plane, with the additional advantage that direct coupling to an Alfvén Wave at the plasma edge is thereby minimised as confirmed experimentally by BORG et al. (1986).

The most strongly excited modes of the fast wave at low frequency are m = -1 in cold plasma MHD, due to the plasma gyrotropy. To excite these modes with low toroidal mode numbers, we use eight external antennae, four above and four below the plasma as shown in Fig. 2. They are electrically floating with respect to the torus wall, and are fed by eight separate buffer amplifiers [LIETTI and BESSON, 1986]. The relative phasing of the antennae defines the

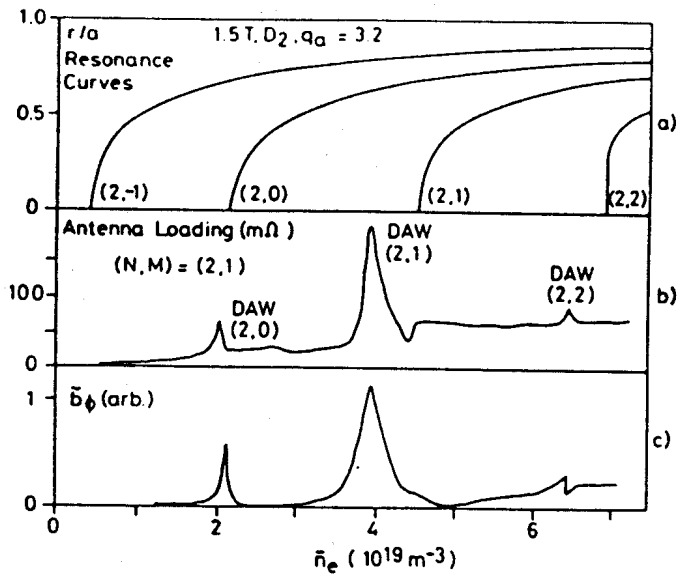

Fig. 1 Illustration of the Alfvén Wave Heating scheme
(a) radial positions of resonance surfaces given by expression (1) for n=2, f_0=2.5 MHz
(b) antenna loading variation measured as a function of density;
(c) externally detected amplitude of the toroidal component of the wavefield.

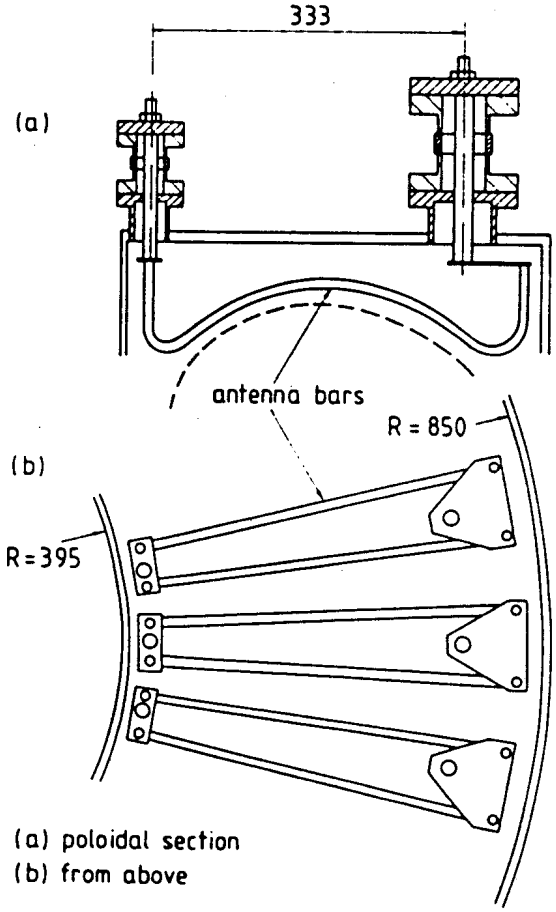

Fig. 2 Illustration of the TCA antenna structure

toroidal mode numbers and the dominant poloidal mode numbers excited. Each antenna, comprising six 10 mm diameter bars fed in parallel, carries an rf current up to 1500 A, with a relatively low applied voltage (± 500 V) due to the large width and low inductance of each antenna together with the low frequency. The antenna bars are coated with TiN, but have also had a whole variety of elements deposited on them during the tokamak discharges. The conductors are unshielded from the plasma, although some experiments have been carried out on TCA with side-screens.

In the remainder of this paper we shall firstly discuss some new results on the excitation of Alfvén Waves, which increase our confidence in the validity of the theoretical models as far as TCA is concerned. The macroscopic effects of the rf power will then be presented with emphasis on these observations, related to changes in the excited spectrum, which indicate changes in the equilibrium current profile.

2. ALFVEN WAVE EXCITATION

A cold plasma 1-D MHD model can be used to describe the driving of the Shear Alfvén Wave resonance, and this was the starting point in Lausanne. Other theory groups have started from a full kinetic treatment in a restricted geometry model. Our 1-D model predicts a value of the antenna loading which is of the order of the measured value, as well as the dominant features. Figure 1(b) shows the measured antenna loading schematically, as a function of the plasma density. The major absorption peak labelled '(2,1)DAW' is described by the model with the inclusion of finite frequency terms and the equilibrium plasma current. This peak is a global eigenmode of the Alfvén Wave, referred to as a Discrete Alfvén Wave (DAW). The other two DAWs require the inclusion of toroidicity [APPERT et al., 1985] in order to be explained. A detailed description of the interpretation of the loading curves and the rf wavefield curves (such as Fig. 1(c)) is to be found in COLLINS et al. (1986). The appearance of a DAW peak, as the density increases, signifies the onset of a new continuum, as can be seen by comparing Figs. 1(a), 1(b).

COLLINS et al. (1986) have already discussed the importance of the plasma equilibrium current in determining the antenna coupling. Here we present some new results on the strength of the excitation of the toroidally coupled (n,m) = (2,0) mode in which we might expect the value of the equilibrium current to play a role in the coupling to the surface wave, and its distribution possibly to be important for the toroidal coupling.

Figure 3 shows the plasma current dependence of the magnitude of the antenna loading in the region around the (n,m) = (2,0) DAW. We have plotted the height of the DAW above the previous continua (ΔR_{pre}, as illustrated in the inset) as well as the height of the DAW above the continua which follow it

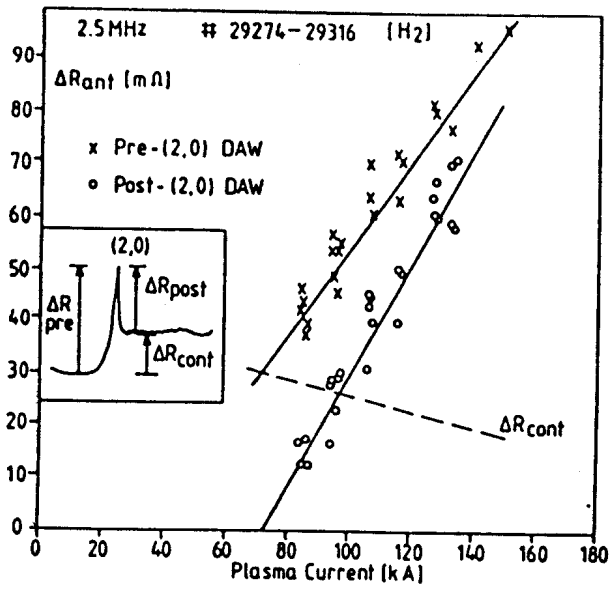

Fig. 3 Coupling to the (n,m)=(2,0) Discrete Alfvén Wave and continuum. ΔR_{pre} corresponds to the amplitude of the DAW loading peak above the previous continua; ΔR_{post} corresponds to that above the following continua; ΔR_{cont} corresponds to the jump in loading when crossing the (2,0) DAW.

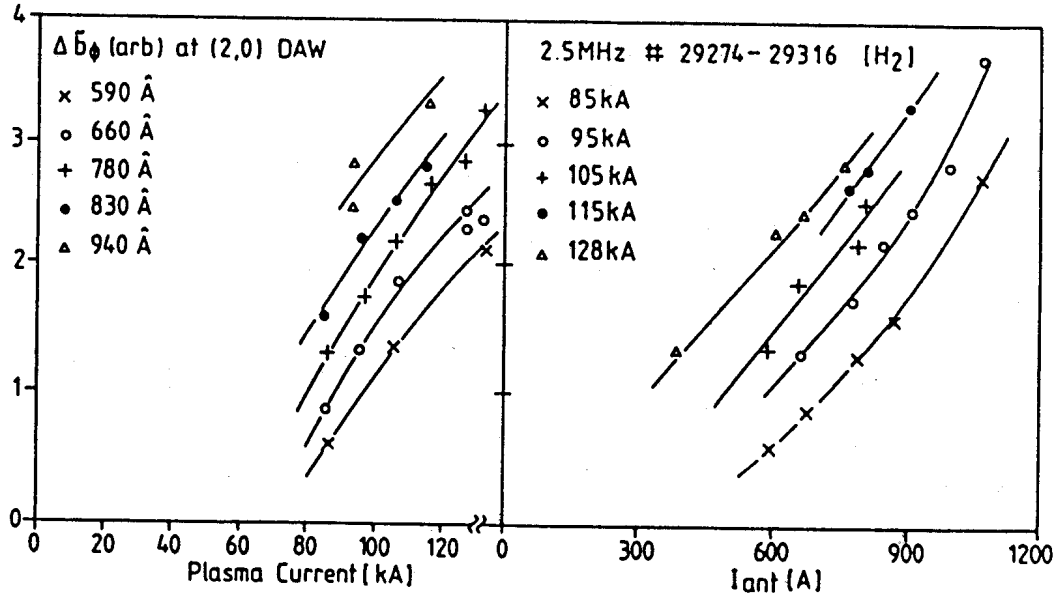

Fig. 4 Strength of the toroidal component of the rf wavefield above the underlying continua as a function of plasma current and rf antenna current.

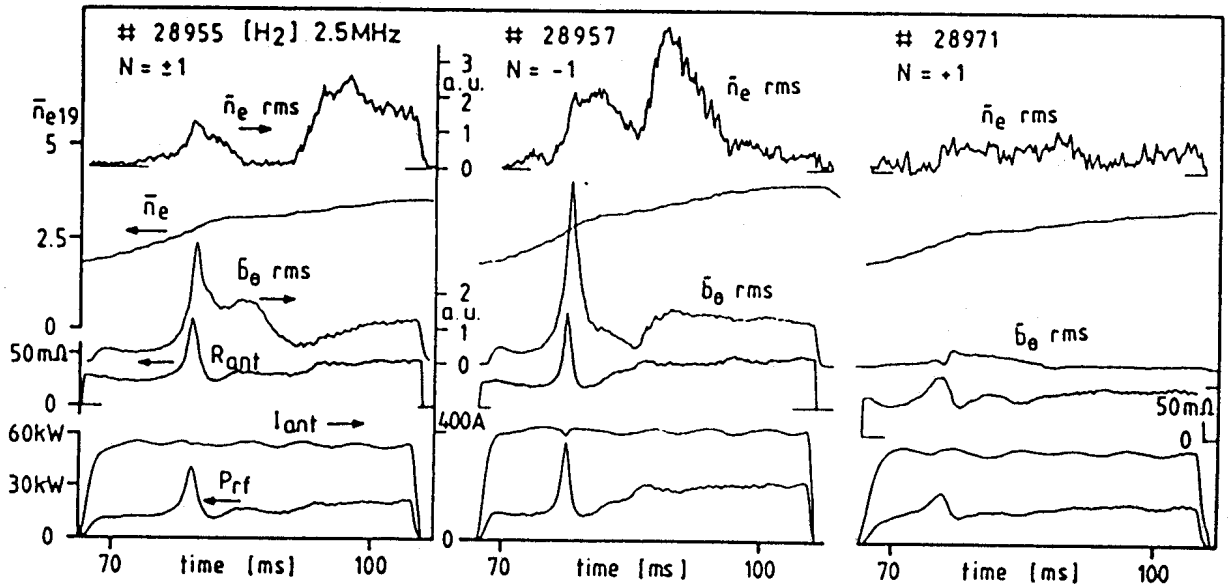

Fig. 5 Amplitude of the driven density oscillations for n=±1, n=+1, n=-1, together with the antenna loading and rf magnetic wavefield [H_2, 15 kG, 2.5 MHz]

(ΔR_{post}). The difference between these two is shown as ΔR_{cont} and is due to the additional contribution of the (n,m) = (2,0) continuum. These measured values are shown in the figure as a function of the plasma current for different antenna currents. Both ΔR_{pre} and ΔR_{post} are strong functions of the plasma current whereas ΔR_{cont} has only a weak, and even opposite dependence. Below a certain plasma current ($I_p \sim 70$ kA, $q(a) \sim 5.5$) the DAW is not visible above the level of the (2,0) continuum, although the jump in the loading due to the new continuum is still measurable. This implies that the role of the equilibrium current differs for the eigenmode and the continuum: the toroidally coupled (n,m) = (2,0) continuum loading is not very sensitive to the value of the plasma current, whereas the (2,0) toroidally coupled DAW requires a significant plasma equilibrium current in order to be excited.

These observations were extended to the measurements of the external rf magnetic wavefield ($\tilde{b}_\phi$). Figure 4 shows $\Delta\tilde{b}_\phi$, the strength of the $\tilde{b}_\phi$ component above the underlying continua, which themselves have an extremely weak $\tilde{b}_\phi$ component in this region of the spectrum. $\Delta\tilde{b}_\phi$ is a strong function of the plasma current and of the antenna current. Below a certain plasma current, $I_p < 70$ kA as before, the (n,m) = (2,0) DAW is not visible on the antenna loading trace for low values of rf antenna current. If the coupling were simply linear, $\Delta\tilde{b}_\phi$ would be a linear function of the rf antenna current for any value of the plasma current, which is clearly not the case at low current. This implies that the rf power is changing the plasma in such a way as to produce the non-linearity. The density profile shape is measured not to be a strong function of the delivered rf power. There is therefore a correspondence between the positive effect of the antenna current (or delivered rf power) and the positive effect of an increased plasma current. The same picture is found when we analyse the $\tilde{b}_\theta$ rf wavefield component for which the amplitude of the DAW signal is less than the underlying continua contributions. These observations are compatible with the interpretations to be discussed later in this paper, that the rf power has an effect on the current profile. A similar argument has been used to explain the 'hysteresis' in the $\tilde{b}_\phi$ signal observed during the rf pulse when the eigenmode resonance was crossed twice [BESSON et al., 1986]. It is not absolutely certain that these effects can be attributed solely to the current distribution in a cold plasma model, or whether the kinetic effects of the DAW itself could be important. The electron temperature on axis varies by nearly a factor of 2 over the range of the plasma current scan. As yet there is no code available which could treat the damping correctly, with full inclusion of kinetic effects, in two dimensions, which would be essential for a complete study of the excitation of the (n,m) = (2,0) eigenmode.

The first observation on TCA which could clearly not be explained in terms of the cold plasma model was the measurement of the driven density fluctuations, whose inward direction of propagation and perpendicular wavelength corresponded to the predictions for the Kinetic Alfvén Wave [HASEGAWA and CHEN,

1975]. These results are described by BEHN et al. (1987) and have now been extended to the case of asymmetrically driven travelling waves.

On TCA we can only preferentially excite travelling waves with n = ±1, due to the number of antennae available. The results are shown in Fig. 5, for similar values of rf antenna current. The antenna loading and external rf magnetic wavefield ($\tilde{b}_\theta$) are strongly reduced for the n = +1 case. Since n/m > 0 (for q(r) positive) for the eigenmodes, this corresponds to strong/weak excitation of m = -1/+1 respectively, as already reported by COLLINS et al. (1986). The upper trace shows the driven synchronous density oscillations integrated along a chord tangential at r/a = 0.55. The strength of this signal is more than 5 times greater for the case (n,m) = (-1,-1) compared with the case (n,m) = (+1,+1), confirming that the measurements made external to the plasma connect with the driven oscillations inside the plasma. These measurements also confirm that the m = -1 preferential excitation of the eigenmode is extended to the m = -1 continuum. The results obtained with different antenna phasings have all shown that the driven oscillations are completely defined by the excitation structure of the antennae.

Ironically, the first evidence that kinetic effects are important was obtained, but not interpreted, long before the direct measurement of the density fluctuations. De CHAMBRIER et al. (1984) noted that the external rf magnetic wavefield phase was not simply explained by the model used. Experiments on PETULA [COLLINS et al., 1986a] documented the strong evolution of the phase beyond the DAW as being a general feature of the rf excitation. Figure 6(a) shows the evolution of the toroidal component of the external wavefield as well as the antenna loading as a function of density in the region around the (n,m) = (2,1) DAW.Figure 6(b) shows the equivalent curves produced from a 1-D model including kinetic effects for the four excited modes (n,m) = (2,1), (2,-1), (-2,1), (-2,-1) [APPERT et al., 1987].

The experimentally measured phase cannot be perfectly modelled by this cylindrical case since the important (n,m) = (2,0) resonance surfaces are not included. For this reason we prefer to replot the rf magnetic wavefield in the complex plane, with the phase defined relative to that of the rf antenna current. In this way, any background wavefield, or even the direct field from the antennae, will appear as a slowly moving offset in the complex plane. Figure 7(a) shows the same experimental data when crossing the (n,m) = (2,1) DAW. The time points marked with arrows in Fig. 6(a) are indicated on the Argand diagram. The vector rotates during the DAW and has two subsidiary rotations afterwards. Figure 7(b) shows the same rotation under the DAW, but no subsequent fine structure in an evolution calculated numerically using the cold plasma model. Figure 7(c) shows the same plot with the inclusion of full kinetic effects. The appearance of the secondary rotations in the complex plane shows a remarkable similarity to the experimental data.

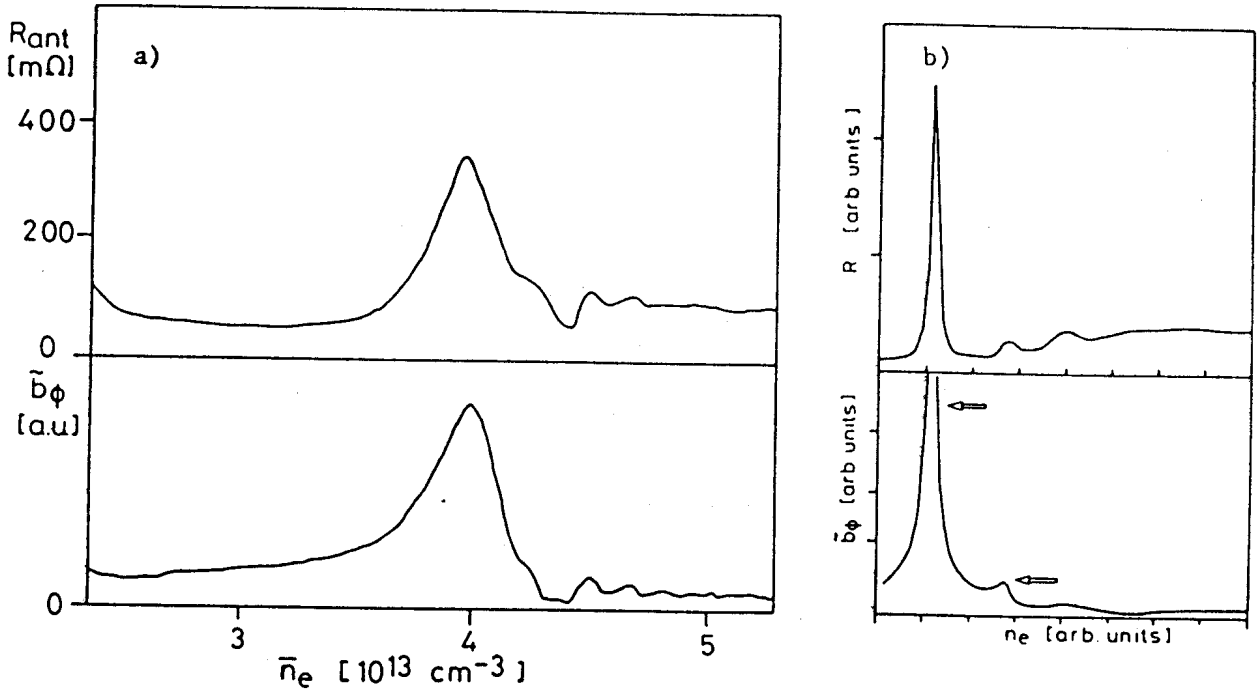

Fig. 6 Antenna loading and rf magnetic wavefield at plasma edge as a function of density (a) experimentally measured; (b) calculated from a 1-D kinetic code.

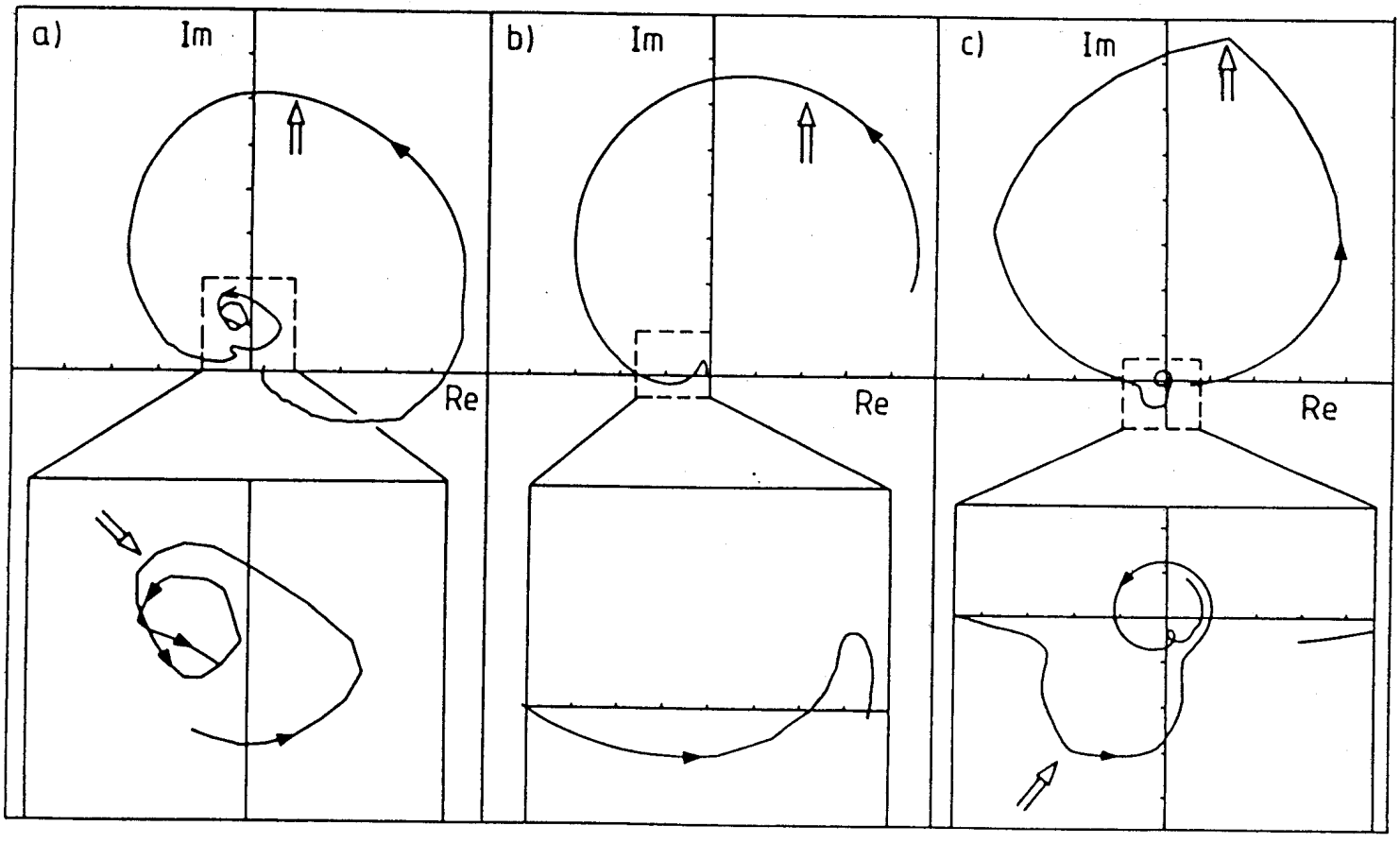

Fig. 7 The rf magnetic wavefield of Fig. 6 plotted in the Argand diagram: (a) experimentally measured; (b) cold plasma model; (c) kinetic model.

These secondary rotations are due to the inward propagation of the Kinetic Alfvén Wave and the consequent possibility of setting up radial standing waves following "reflection" at the axis. HASEGAWA and CHEN (1976) already saw that such a standing wave would change the antenna-plasma coupling from the cold plasma calculation, otherwise valid even when kinetic effects are included. Numerical simulations of these features in 1-D have previously been carried out by DONNELLY et al. (1985), ELFIMOV et al. (1980) and ROSS et al. (1982). Figure 6(a) shows small peaks in the antenna loading and the external rf magnetic wavefield after the DAW which correspond to the rotations in the complex plane. Such peaks in the rf wavefield were attributed earlier [DE CHAMBRIER et al., 1982] to higher radial modes of the DAW below the continuum threshold in the cold plasma model; we must now attribute them to kinetic effects which destroy the sense of the continuum threshold, and move the resonance frequencies of the satellite peaks into the frequency domain of the cold plasma continuum. This is only seen for modes with $m/nq > 0$.

The point in the spectrum at which the external rf magnetic wavefield no longer has any fine structure will therefore correspond to the point at which the Kinetic Alfvén Wave has a relatively small amplitude at the axis. This external 'measurement' is thus an indication of the power deposition profile! The extent to which the Kinetic Alfvén Wave is observed to reach the axis supports the hypothesis made earlier to explain the large electron temperature sawtooth amplitude during Alfvén Wave Heating on TCA [JOYE et al., 1986].

By analogy with the 'internal' standing wave, an 'external' standing wave could be set up, between the resonance layer and the edge (Surface Quasi-Electrostatic Wave). The amplitude of these resonances was predicted to be very large, of the order of the DAW resonance loading, but no experimental evidence for them has been found on TCA. The reason for their non-existence may lie in the collisionality at the edge [APPERT et al., 1987] or in the diffuse nature of the edge profiles [DONNELLY et al., 1986].

Let us now summarise this section. The new results obtained concerning the effects of kinetic terms on the theoretical predictions for the measurable quantities are fully supported by the new experimental measurements presented. The importance of the kinetic effects is now even clearly documented in the measurements made outside the plasma column. This leads to an increased confidence in the predictions of such a kinetic model, especially in the validity of the calculated power deposition profiles. The dependence of the external rf magnetic wavefield on the antenna current suggests, however, that the rf power considerably perturbs the plasma response, leading to a non-linear dependence. A small redistribution of the plasma current may be at the root of this observation. The increased understanding of the wave launching will help us to interpret some of the effects of the rf power in terms of the predicted power deposition.

3. EFFECTS OF THE RF POWER ON THE PLASMA

Having looked at the launching of Alfvén Waves in TCA, we now turn to the effects of the rf power on the plasma. Several of these effects will be discussed in this section, namely: the increase in density, the increase in plasma energy, the variations in $\beta+li/2$, Rpl and $\beta_\perp$ as the excited spectrum evolves, changes in the MHD activity and finally some remarks on rf power modulation experiments.

3.1. Density rise

During the Alfvén Wave Heating experiments on TCA there has always been a density rise. In the simple examples, the density rise is smooth, and, with the gas valve voltage clamped at the level before the rf pulse, the density tends towards a new equilibrium. From bolometric measurements the maximum influx of high Z impurities was concluded to be insufficient to explain the electron density rise. Due to the simple form of the density rise a model was proposed in an attempt to quantify the effect. The rate of change of the line-integrated electron density is taken to be the sum of two linear terms as shown in Fig. 8, thus :

$$dn_e/dt = -G(n_e - n_{eo}) + SF$$

where the gain and source coefficients G and S are constants, (n_e-n_{eo}) is the difference in density from the start of the rf pulse, and F is an as yet unspecified source functional dependence. We assume that the plasma has a stationary density before the rf pulse is applied.

To identify the best functional dependence for F, among reasonable hypotheses, we took different trial functions of rf parameters, eg : antenna current, antenna current squared and the delivered rf power. The delivered power was found to work best in that a good deal of the temporal structure in the rf power trace was required to produce a good fit to the density rise. This is already surprising since the power radiated from the antenna is not local to the antenna structure. Any local antenna - edge-plasma interaction might be expected to vary as I_{ant} or I_{ant}^2, in a non phase-coherent manner. These two trial functions both gave very poor fits.

The constants n_{eo}, G and S were fitted using the least squares method. The ratio S/G was constant to within a factor of two for a series of supposedly reproducible shots. Closer re-examination of the raw data in fact allowed a separation of the shots into classes within which the S/G ratio was constant to 20%. Thus, the fit procedure was able to distinguish between similar shots which showed only minor differences in plasma parameters.

These fit parameters were evaluated for an rf power scan and a plasma

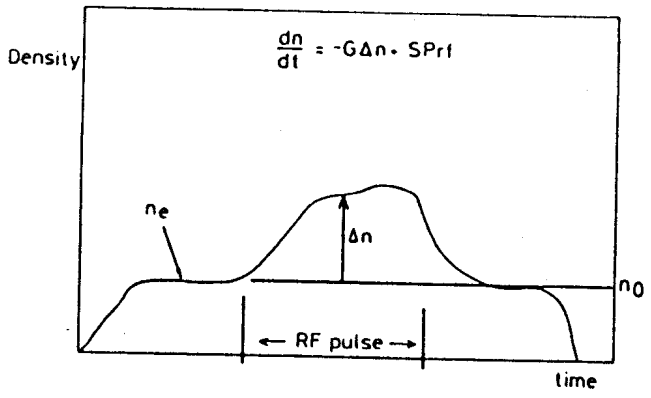

Fig. 8 Schematic of a typical density evolution during a plasma discharge indicating the density fit parameters.

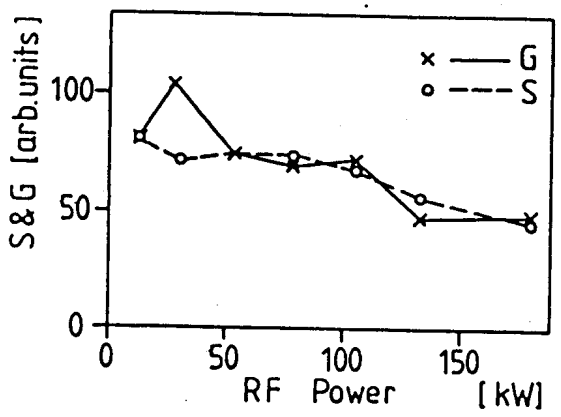

Fig. 9 Density rise coefficients for a rf power scan.

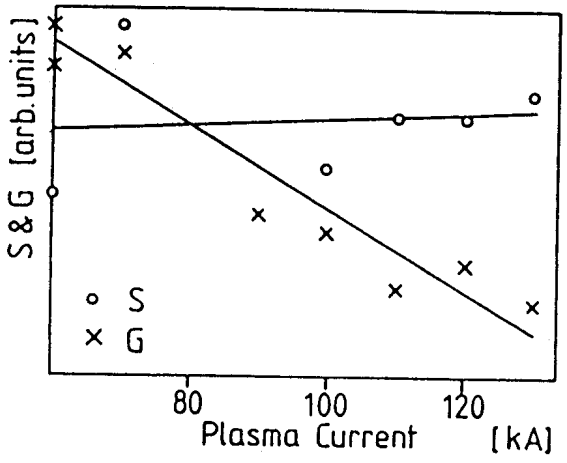

Fig. 10 Density rise coefficients for plasma current scan.

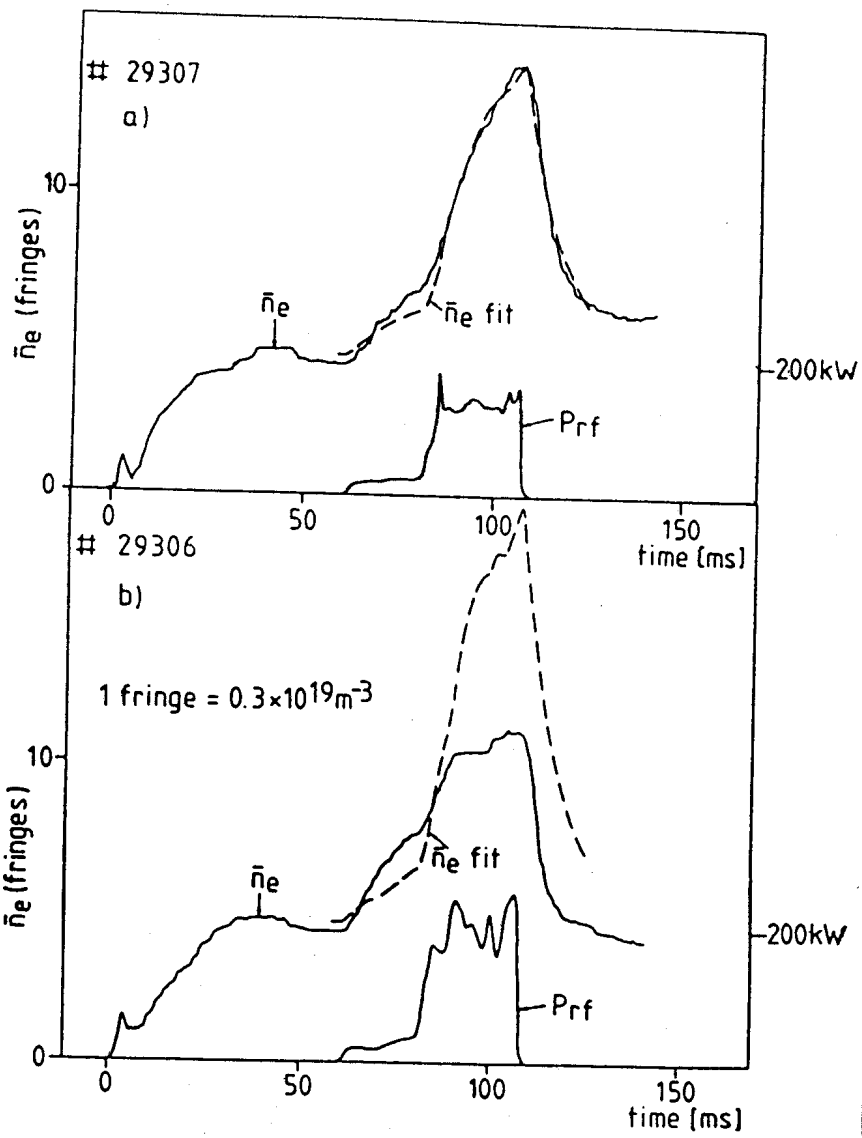

Fig. 11 Density evolution for two nominally similar discharges

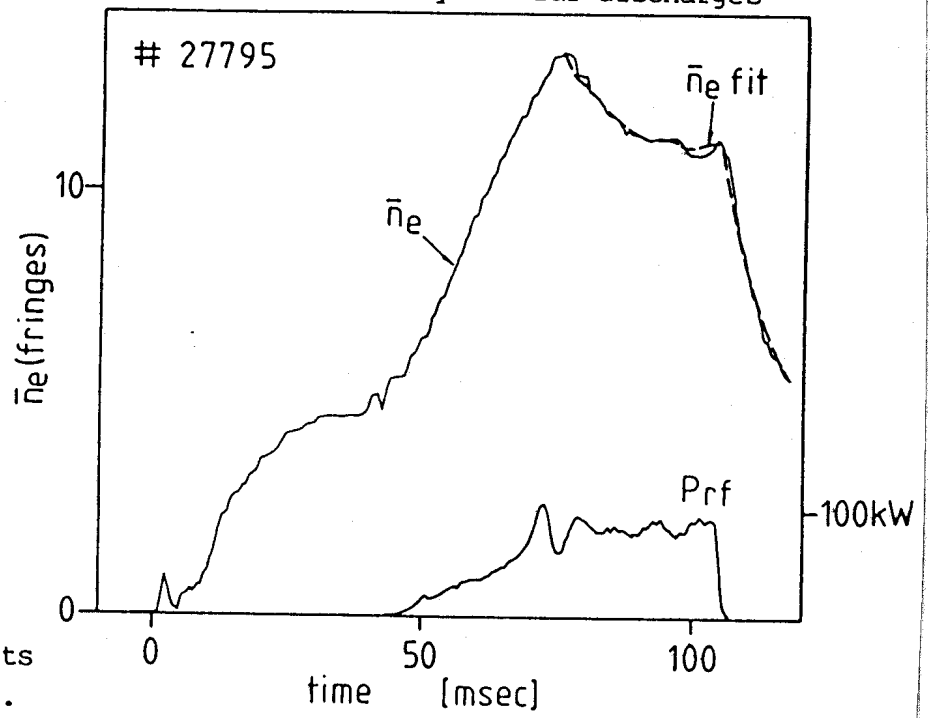

Fig. 12 Density evolution for a shot in which a discontinuity occurs near a DAW.

current scan. For Fig. 9, the rf power was varied from 10kW to 180kW. Although this did not include the highest powers reached on TCA, it covered the range of power easily accessible. S and G did not change by more than a factor of 2 over the complete range for over an order of magnitude change in the delivered rf power, indicating that the density rise is nearly proportional to the rf power. The ratio S/G was again constant to within 20%. Since the S and G coefficients tend to correlate, the ratio S/G gives a better parameterisation of the shot, and the absolute values of S and G change the shape of the fitted density rise more than its absolute value. Figure 10 shows the fit parameters for a series of shots with different plasma currents. Whereas the S parameter remained constant through the current scan, the G parameter decreased with increasing plasma current. Since S remained constant, we conclude that the rf power acts as a "pure source" of plasma particles, and the change in G reflects the improved particle confinement often observed with increasing plasma current in tokamaks. There is no difference observed between the radial density profile with or without rf, at the same density.

The simple model proposed to parameterise the density rise has therefore shown the following properties :

1) It gives reproducible coefficients for a large range of rf powers.
2) The S term stays constant when the particle confinement changes as a result of a change in the plasma current.
3) The fit parameters can be used to distinguish discharges which show only minor differences in other plasma parameters.

The density does not always evolve in such a smooth and predictable manner, and discontinuities in the density rise have been observed. Two examples of this type of behaviour are described, chosen because the effect on the density evolution is dramatic, although less remarkable on other measurements.

In the first example, the density evolution of two nominally similar discharges is contrasted. The density rise in Fig. 11(a), is well fitted by the simple model. Using the same coefficients obtained from this fit, the predicted density rise is shown in Fig. 11(b) for a discharge in the same series. The density clearly undershoots the calculated curve, at which time there is some modulation of the H_α signal indicating a reluctance of the plasma to accept a higher density.

In the second example, Fig. 12, the density evolution shows a break in the density rise ~80ms into the discharge. The density rise model is clearly inappropriate up to this break since the density rises almost linearly with time, independently of the changes in the rf power. In fact the plasma density increases much faster than would have been expected from the coefficients of the first fits presented. After the discontinuity, the plasma density relaxes

to a lower level, although the rf power remains roughly constant, and then decays at the end of the rf pulse. After the break, and including the period after the rf pulse, the density is well described by the model, with coefficients S and G which are consistent with "normal" discharges. Here the plasma appears to have gone through an internal change and then relaxed into another state. In this case, it is the state before the discontinuity which seems to be unusual, whereas the new state, in which the plasma remains until the end of the discharge, is consistent with "normal" discharges. This discontinuity usually occurs close to a Discrete Alfvén Wave, coinciding with the onset of a new continuum threshold. This type of behaviour can also be provoked, during the rf pulse, by a sudden increase in the m=2 MHD activity, unrelated to the appearance of a new continuum.

To summarise, this first attempt to quantify the density rise accompanying the rf heating on TCA has shown that a simple 0-D model in which a source of particles proportional to the rf power can fit the observed density rise remarkably well. Although many different electron density evolutions are observed, it is hoped that a simple change in the transport coefficients may be sufficient to explain the effect. So far, no mechanism for the density rise has been identified, although YASSEEN and VACLAVIK (1986) have proposed a direct rf pump as a candidate.

3.2. Rf heating

Results on ion-heating have been reported already [DE CHAMBRIER et al. 1983] and only show a small effect (<2 eV10^{19}kW^{-1}m^{-3}) above the increase expected as a result of the increased density. Thomson scattering measurements showed an extremely strong electron temperature sawtooth excursion ($\Delta Te(0)/Te(0)$ ~50%) but only a small change in the baseline temperature [JOYE et al., 1986]. In both these cases the interpretation is complicated by the large density rise.

Here we present some global quantities, uncorrected for the rate of change of density. In Fig. 13 we show the maximum value of $(\beta+li/2)$, calculated from the plasma equilibrium, obtained during the rf pulse with different values of rf antenna current and plasma current. We note that $(\beta+li/2)_{max}$ is greatest (~1.48) at low current ($q(a)$~5.5) and that it flattens off as a function of rf antenna current. $(\beta+li/2)$ increases from 0.90 to 1.48 with only 160 kW of rf power. If this increase were all due to a change in β, we would deduce an energy confinement time of 7.6 msec., in excess of the ohmic value.

The results of the diamagnetic measurement of $\Delta\beta_\perp$ are far noisier. Nonetheless Fig. 14 shows the same trend, in that $\Delta\beta_\perp$ is larger for lower values of plasma current but it increases more steadily as a function of the delivered rf power. An estimate of $\tau_{inc}=\Delta W/(\Delta P_{oh}+P_{rf})$ gives values between 1.7 and

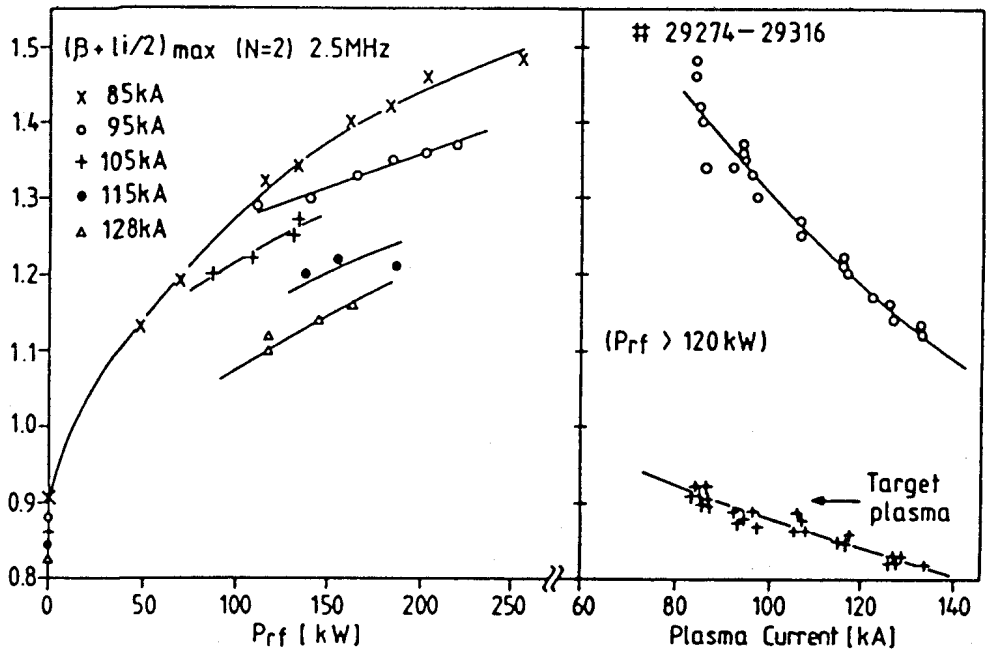

Fig. 13 Maximum value of (β+li/2) obtained for different plasma currents and different rf antenna currents.

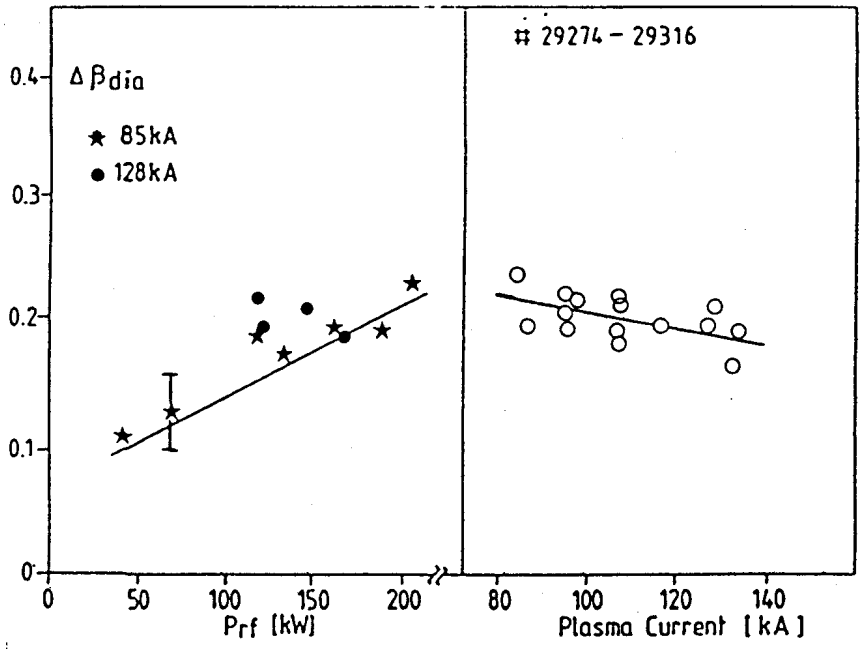

Fig. 14 $\Delta\beta_\perp$ during the rf pulse as a function of plasma current and delivered rf power.

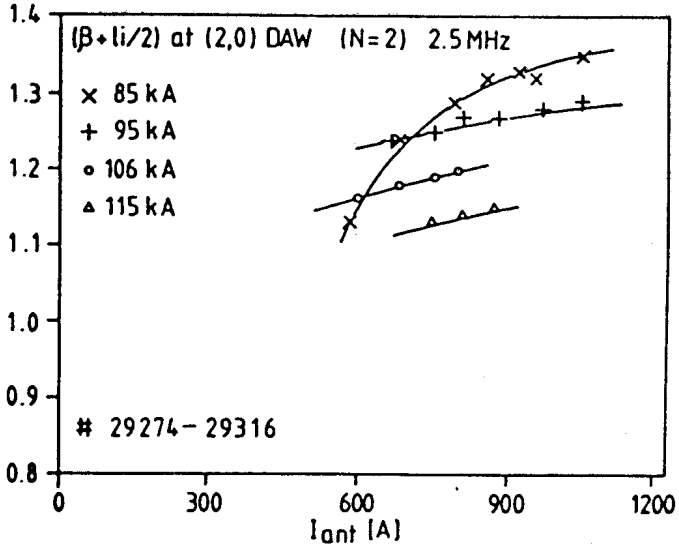

Fig. 15 Variation of (β+li/2) at fixed spectral condition ((n,m)=(2,0)DAW) as a function of rf antenna current.

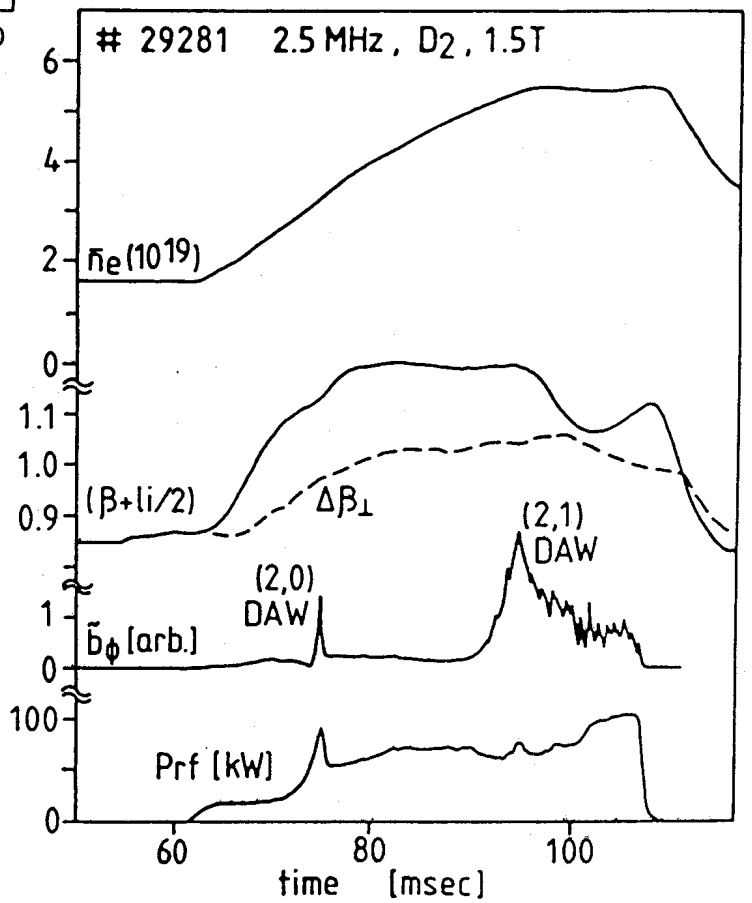

Fig. 16 Temporal evolution of (β+li/2) and $\beta_\perp$ when a spectral threshold is crossed.

3.0 msec, of the order of the ohmic confinement time. The noise on $\Delta\beta_\perp$ does not allow a direct comparison to confirm or contest the degree of confinement degradation.

Since much of the increase in $(\beta+li/2)$ could be due to the density increase, we have plotted in Fig. 15 the variation of $(\beta+li/2)$ as a function of rf antenna current at the instant the $(n,m)=(2,0)$ DAW is crossed, corresponding to a fixed density. There remains an increase with delivered rf power.

The difference between $\Delta(\beta+li/2)$ and $\Delta\beta_\perp$ suggests that there is a significant change in the internal inductance, up to a maximum of $\Delta li \sim +0.6$, which would have to correspond to a significant change in the plasma current distribution.

Such a global analysis, ignoring the evolution of the plasma parameters, conceals the rôle of the Alfvén Wave spectrum in determining $\Delta(\beta+li/2)$ and $\Delta\beta_\perp$. Figure 16 illustrates the evolution of both quantities. After crossing the $(n,m)=(2,1)$ DAW, both $(\beta+li/2)$ and $\Delta\beta_\perp$ decrease, although the delivered rf power increases. The value of $(\beta+li/2)_{max}$ is therefore obtained with a delivered rf power much less than the maximum delivered. The maximum value of $(\beta + li/2)$ is nearly always reached close to the (2,0) DAW for low density target plasmas. It is clear that the value of τ_{inc} must be varying considerably during the rf pulse, according to the part of the Alfvén Wave spectrum excited, or the exact form of the deposition profile. Unfortunately $(\beta+li/2)$ increases so rapidly during the first "efficient" phase before the first eigenmode is crossed, that the analysis depends too strongly on the time derivatives in the power balance. We have not yet been able to stabilise the discharge during this phase of the rf pulse.

3.3. Fine effects of the excited spectrum

In this section we look more closely at the fine effects relating to the excited spectrum. The rise in the density, although limiting our power levels, provides us with the fine resolution during the evolution of the excited spectrum. Such a fine resolution could never be achieved on a shot-to-shot basis. We have already noted the effect on the density rise, and now consider $(\beta+li/2)$ and $R_{pl}=(V-L_p dI_p/dt)/I_p$ where L_p is fixed and does not take into account any change in li. We already showed [BESSON et al., 1986] that a dip in R_{pl} occured at a fixed position relative to the DAW and Fig. 17 illustrates this in detail as a function of the plasma current. Both a dip in R_{pl} and a break in $(\beta+li/2)$ are seen after the (2,0) DAW for low and high values of the plasma current.

For Fig. 18, we varied the excitation conditions, crossing the

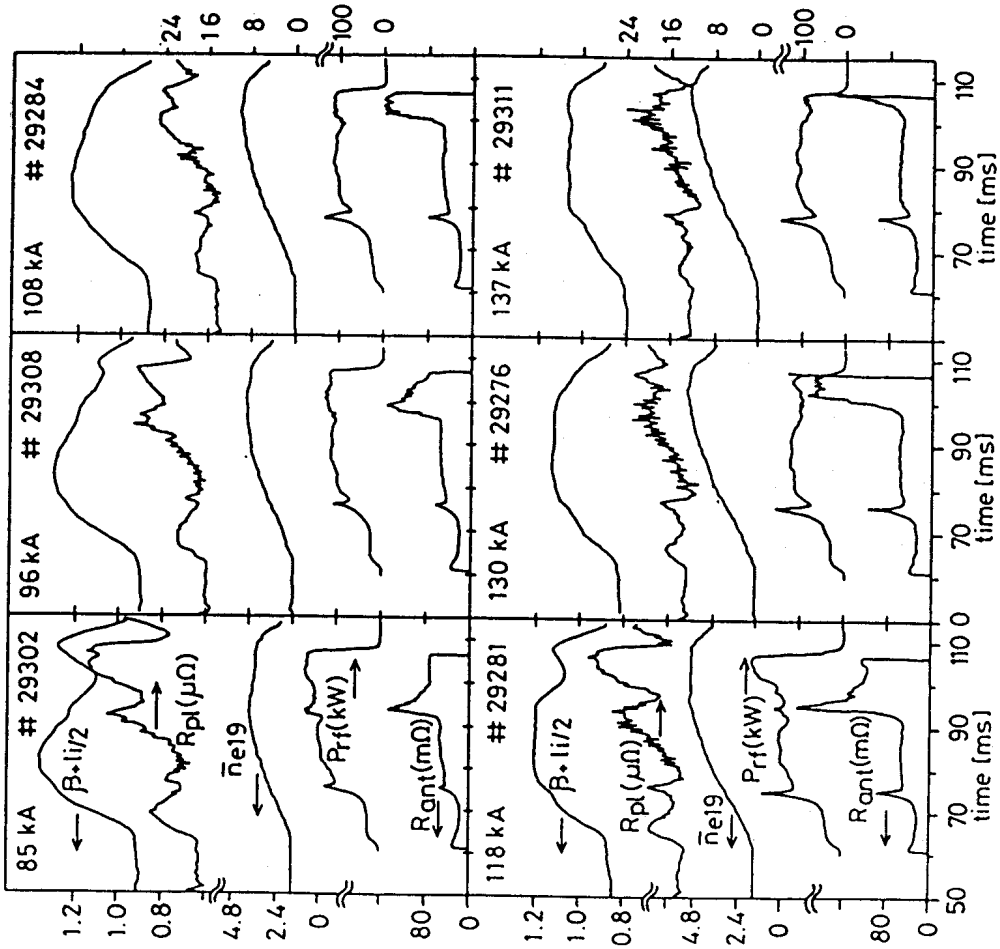

Fig. 17 Evolution of (β+1i/2) and R_{pl} for different plasma currents [D_2, 1.5 T, 2.5MHz, N=2]

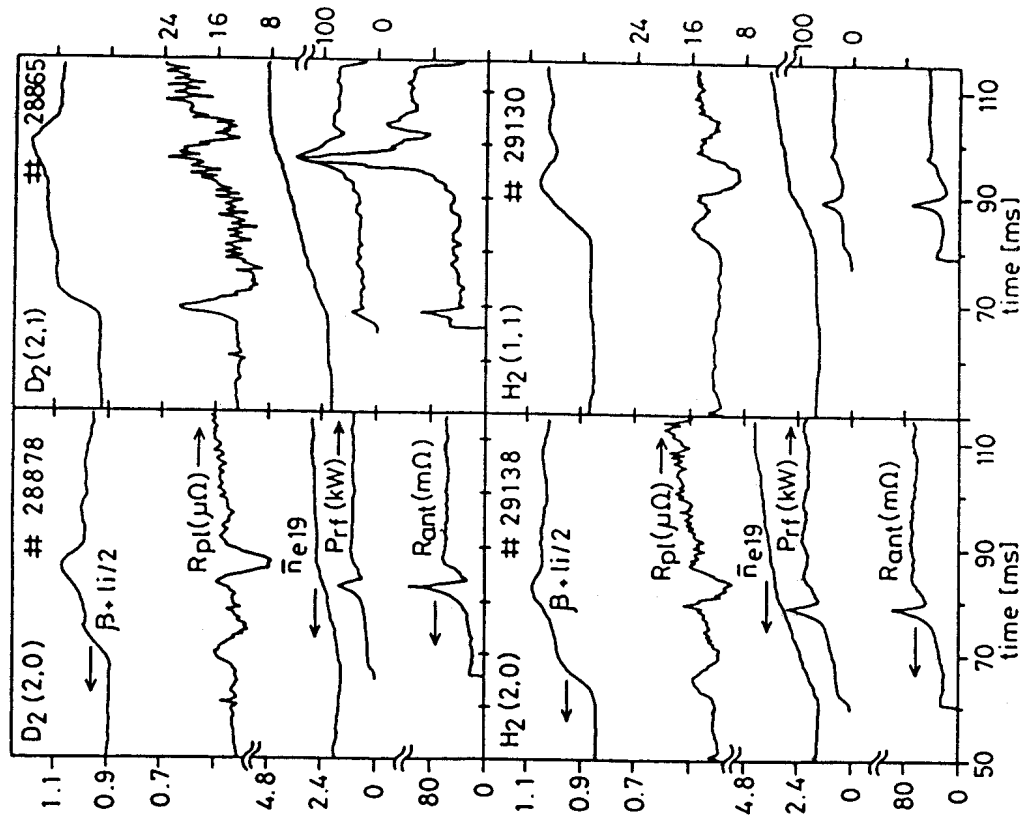

Fig. 18 Evolution of (β+1i/2) and R_{pl} for different excitation structure (I_p=130kA) [1.5T, 2.5MHz]

(n,m)=(1,1)DAW (H_2), (2,0)DAW (H_2), (2,0)DAW (D_2) and (2,1)DAW (D_2), at fixed plasma current (I_p~130kA). The dips in (β+li/2) and R_{pl} remain associated with the arrival of the new continuum threshold (Fig. 1(a), (b)). When a threshold is crossed, the radius of the next outermost resonance surface varies for the different modes (n,m)=(1,1), (2,0), (2,1), and so the dips in (β+li/2) and R_{pl} are clearly not identifiable with these resonance surfaces.

When exciting n=1 waves we can preferentially excite n=+1 or n=-1 as already mentioned. At fixed antenna current, the direction of propagation of the wave does not determine the presence of the dip, eliminating an effect due to direct current drive [Fig. 19].

It is difficult to attribute the dip in R_{pl} to a resistive change, since the soft X-ray flux does not show a strong simultaneous effect at the centre. The parameter R_{pl} also contains a d(li)/dt term and the most likely explanation is that the effect is inductive in origin. This would also explain why we do not see a more and more pronounced effect as the delivered rf power is increased, since we cannot reasonably expect li to keep changing linearly.

Why does li decrease at the Alfvén spectral thresholds? Since this decrease is with respect to a value of li which is already greater than the ohmic one, we might attribute the change to a redistribution of the delivered rf power. When the excited spectrum changes and the loading increases, at fixed delivered rf power, the power in the outer resonance surfaces, which had produced an increase in li, is reduced, in favour of the new inner resonance surface. This logic would imply that the DAW itself would have the most effect, by virtue of its high loading, which is not the case. Alternatively, the new power deposition profile, perhaps concentrated between q=1 and q=2, may cause an ohmic (i.e. conductivity) change in the profile. It is clearly most unsatisfactory that the mechanism is not yet identified.

3.4. Effect on the MHD activity

Applying the rf pulse changes the MHD activity, measured as the m=even component of the Mirnov activity $|\tilde{B}_\theta(a)|$. When the activity increases, it can reach a threshold value beyond which a disruption occurs, thereby limiting the rf power delivered. The detailed behaviour of the MHD signal is strongly linked to the Alfvén Wave spectrum, as previously reported by BESSON et al., (1986), resulting in an enhanced probability of a disruption at or close to a spectral threshold, for a given rf power level. This is illustrated in Fig. 20.

The delivered power can be substantially increased, by over a factor of 2, between the spectral thresholds. At this increased power level, the density will rise to provoke the crossing of the next threshold, leading inevitably to

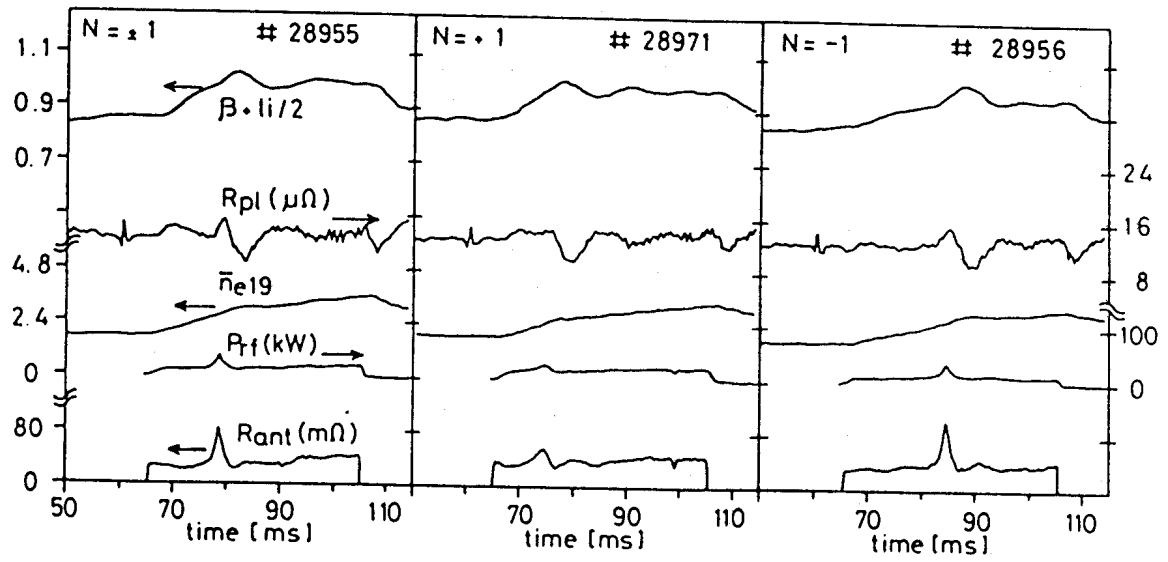

Fig. 19 Evolution of $(\beta+li/2)$ and R_{pl} for different direction of excited travelling waves, n=±1, n=+1, n=-1. [H_2, 1.5T, 2.5MHz]

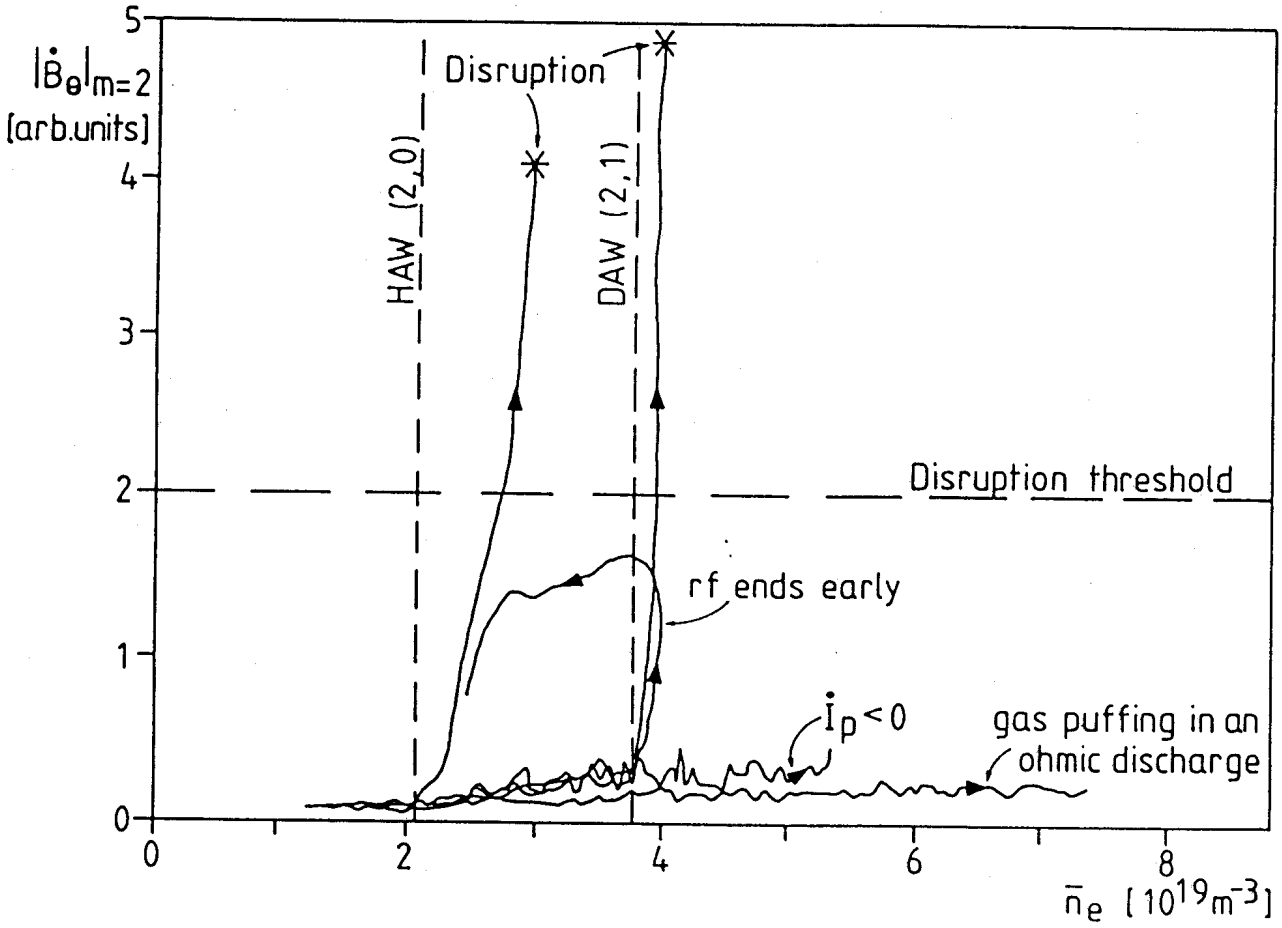

Fig. 20 Schematic of the MHD activity leading to a disruption close to an Alfvén Wave spectral threshold.

an increase in the MHD activity and a disruption. The level of MHD activity at which the disruption is inevitable is similar to that with ohmic heating alone, suggesting the same self-destabilizing mechanism as in the ohmic case. The question is therefore reduced to why the MHD activity increases in the first place. The sensitivity to the delivered rf power is reduced in higher q(a) discharges, and also if $dI_p/dt<0$.

Two possible causes of the increase in MHD activity are a local increase in $|dj(r)/dr|$ near q(r)=2 and an increase in the global gradient between q=1 and q=2 leading to coupled destabilisation at rational q(r) surfaces, as described by BONDESON (1986). A change in the m=2 MHD activity has already been reported in ECRH experiments by Alikaev et al. (1985) and we therefore consider the MHD activity increase during rf heating to be due to changes in the power desposition profile combined with changes in li as already documented. We therefore investigate the evolution of the MHD activity in detail for different conditions.

The amplitude of the MHD modes is changed by the rf pulse, either increasing or decreasing relative to the ohmic level, according to the part of the spectrum excited. This is documented in Fig. 21(a), (b), (c) representing the time evolution of the loading of the antenna (R_{ant}) and the Mirnov signal. Although we measure routinely the m=even modes, more detailed measurements have shown that the signal from the m=2 n=1 mode dominates. The effect of the wave on the mode activity is illustrated by two series of shots at fixed plasma currents (85kA and 135kA) for different rf powers (Fig. 21(a), (b)) and the link between them is made by showing a plasma current scan at roughly constant antenna current.

Firstly, an overview of the possible effects is given in Fig. 21(a), with I_{ant} ~750 A. Shortly after the start of the rf pulse the (2,-1) continuum causes a factor of 3 decrease in the MHD signal relative to the ohmic level. A sudden increase occurs at the (n,m)=(2,0)DAW followed by a slight decrease in the (2,0) continuum. Another sharp peak appears at the (2,1)DAW followed by a clear decay back to the ohmic level. Finally the (2,2)DAW induces a strong but short peak after which the signal returns to 2/3 of the ohmic level. The end of the rf pulse produces a burst of activity which cannot be analysed here since the plasma current flat top ends shortly afterwards. All these features are general and are found in the other traces of Fig. 21 with different degrees, depending on the values of plasma current and rf power. The signal drop in the (2,-1) continuum disappears at high current probably mainly due to the fact that the ohmic level is lower at higher plasma current. The increase in the activity in the continuum, shortly before the (2,0)DAW, is a feature of the low power or high plasma current shots.

The increase in activity near the DAW's is a dramatic effect causing the

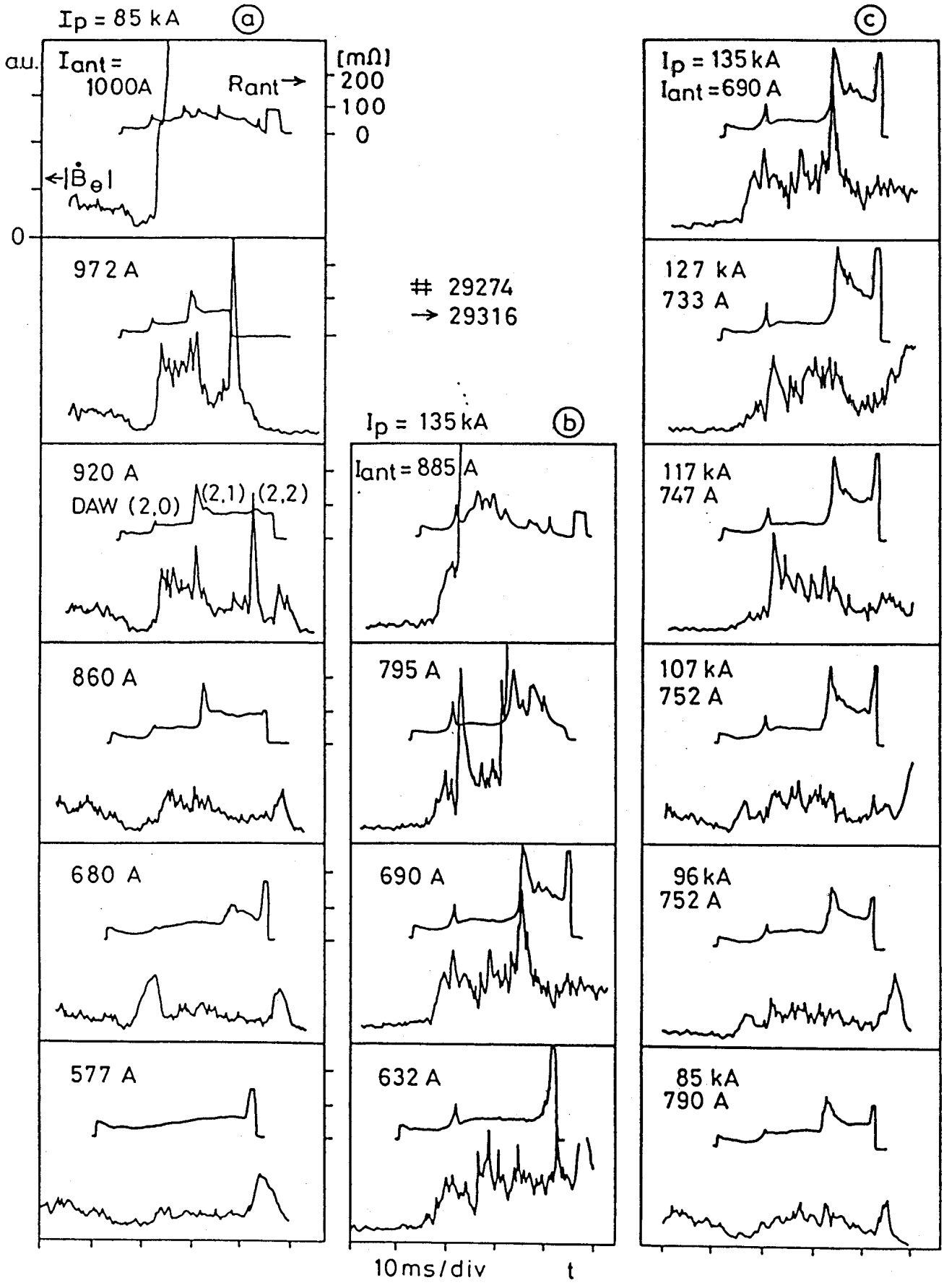

Fig. 21 Effect of the Alfvén Wave spectrum on the MHD activity. The different curves are aligned vertically on the (2,0) DAW. Therefore, the time scales are slightly translated and the starting points are 50 ± 3 ms. [1.5T, H_2, N=2, 2.5MHz]

plasma to disrupt at high rf power as already mentioned (Fig. 21(a) and (b)). At plasma currents higher than 115kA the disruption occurs at a lower rf power for the (2,1)DAW than for the (2,0)DAW. At lower values of plasma current these cases cannot be clearly separated.

In the power scan it clearly appears that the effects of the DAW's increase nonlinearly with the antenna current, in agreement with the nonlinearity of their amplitudes, as already discussed. This fact may indicate that the power deposition plays a role in the mode stability via the current profile. This trend also appears in the plasma current scan, but less clearly, probably due to the influence of q(a) on the mode stability. Nevertheless the plasma current scan is surprisingly similar to the rf power scan at 85kA. The cross linking between plasma current and antenna current is again reminiscent of the results of the wavefield strengths.

This study has shown that the rf power is able to stabilise or destabilise the MHD activity and that this is clearly related to the excited spectrum. This particular series of shots shows that a large part of the "fine" temporal structure of $|B_\theta|$ is reproducible, revealing the existence of a complex and subtle balance between the influences of the different parts of the spectrum, the strength of each part being dependent of the antenna and plasma current. When the working gas is changed, the density at which these changes occur remains linked with the spectrum.

It is not possible to say whether the energy deposition profile or local current drive is the cause of the current profile change, although the travelling wave experiments showed no dramatic change in the MHD activity between n=+1 and n=-1 excitation.

4. MODULATION OF THE RF POWER

Many of the observations already described could be attributed to changes in the power deposition profile as the excited spectrum evolves. In order to try to determine this profile, and to examine the transport changes during the rf pulse, we have started experiments with an amplitude modulation of the rf power.

Figure 22 shows preliminary results from these experiments, in which the modulation frequency was varied from 100-500 Hz, with a peak to peak power modulation depth of the order of the mean level. The phase and amplitude of the response of the 15-channel soft X-ray detector and 8-channel FIR interferometer were analysed digitally. The sampling time necessary at the frequencies used precluded any temporal resolution during the rf pulse. The radial profile of the amplitude and phase of the soft X-ray response is very different from that

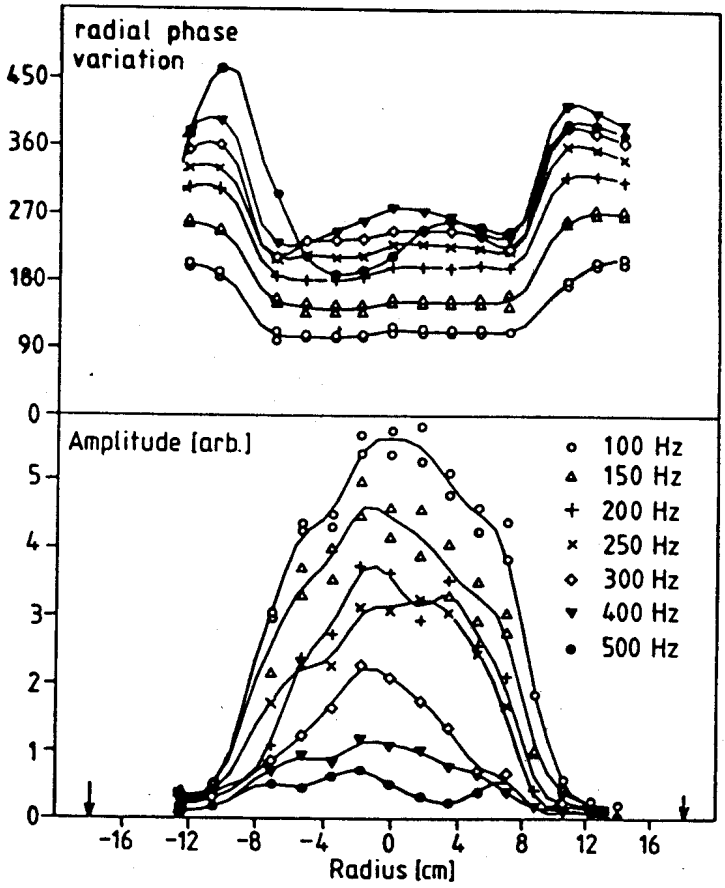

Fig. 22 Response of the soft X-ray to the modulation of the rf power.

of the electron-density response, indicating that the soft X-ray response mostly represents a temperature modulation. The radial dependence of the phase shift with respect to the antenna current shows a hollow profile at the highest frequencies, indicative of an off-axis power deposition profile, near $q = 1$, but averaged over the evolution of the Alfvén Wave Spectrum. The jump in phase between $r = 7.5$ and 10.5 cm indicates a good confinement region, although the spatial resolution must be improved. Analysed with a slab model and assuming a constant $n_e\chi_e$, the propagation of the heat pulse in this region allows us to estimate χ_e. The spread of data for the different frequencies suggest values of χ_e between 0.2 and 0.4 m^2sec^{-1}, comparable, within their accuracy, with ohmic values derived from a radial power balance analysis.

5. CONCLUSION

The experimental results on the antenna loading and the rf wavefield are described even in fine detail if we take into consideration all the effects of the plasma equilibrium current, plasma gyrotropy, toroidicity and plasma temperature. Since the experimental results reflect so accurately the main predicted features due to these effects, we can believe that the predicted energy deposition profile may also be correctly modelled.

Many of the plasma parameters which we can measure show temporally discontinuous behaviour when the excited spectrum changes suddenly at a new Alfvén Wave threshold, and we attribute these observations to the consequent changes in the deposition profile. The behaviour of all these discontinuities would be compatible with a change in the distribution of the plasma current. It is now widely considered elsewhere that this current profile cannot be altered, even in the presence of strong additional heating. It is therefore most unfortunate that one of the dominant features of our experimental data should be both of such interest and unproven by a direct measurement of $j(r)$.

ACKNOWLEDGEMENTS

We would like to acknowledge many stimulating discussions with Professor A. Bondeson and we thank the TCA support team for their continued enthusiasm. This work was partly supported by the Fonds National de la Recherche Scientifique.

REFERENCES

V.V. Alikaev and K.A. Razumova, Course and Workshop on Applications of RF Waves to Tokamak Plasmas, Varenna, Vol. 1, 377 (1985).

K. Appert, G.A. Collins, F. Hofmann, R. Keller, A. Lietti, J.B. Lister, A. Pochelon and L. Villard, Phys. Rev. Lett. 54, 1671 (1985).

K. Appert, T. Hellsten, O. Sauter, S. Succi, J. Vaclavik and L. Villard, Comput. Phys. Commun. 43, 125 (1986).

K. Appert, T. Hellsten, H. Lütjens, O. Sauter, J. Vaclavik and L. Villard, this conference.

R. Behn, A. de Chambrier, G.A. Collins, P.-A. Duperrex, A. Heym, F. Hofmann, Ch. Hollenstein, B. Joye, R. Keller, A. Lietti, J.B. Lister, J.-M. Moret, S. Nowak, J. O'Rourke, A. Pochelon and W. Simm, Plas. Phys. and Contr. Fusion 26, 173 (1984).

R. Behn, G.A. Collins, J.B. Lister and H. Weisen, Plas. Phys. and Contr. Fusion 29, 75 (1987).

G. Besson, A. de Chambrier, G.A. Collins, B. Joye, A. Lietti, J.B. Lister, J.-M. Moret, S. Nowak, C. Simm and H. Weisen, Plas. Phys. and Contr. Fusion 28, 1291 (1986).

A. Bondeson, Nucl. Fusion 26, 929 (1986).

G.G. Borg, M.H. Brennan, R.C. Cross, J.A. Lehane and A.B. Murphy in Proc. of the 13th European Conference on Contr. Fusion and Plasma Heating, Schliersee, Vol. 10C, Part II, 52 (1986).

A. de Chambrier, A.D. Cheetham, A. Heym, F. Hofmann, B. Joye, R. Keller, A. Lietti, J.B. Lister, A. Pochelon, W.C. Simm, J.-L. Tominato and A. Tuszel in Proc. of the Third Joint Varenna Grenoble International Symposium on Heating in Toroidal Plasmas, Grenoble, Vol. 1, p. 161 (1982).

A. de Chambrier, G.A. Collins, P.-A. Duperrex, Ch. Hollenstein, R. Keller, A. Lietti, J. O'Rourke, A. Pochelon and W. Simm, Helv. Phys. Acta 57, 110 (1984).

G.A. Collins, F. Hofmann, B. Joye, R. Keller, A. Lietti, J.B. Lister and A. Pochelon, Phys. Fluids 29, 2260 (1986).

G.A. Collins, A.A. Howling, J.B. Lister and Ph. Marmillod, Lausanne report, LRP 294/86 (1986a).

I.J. Donnelly, B.E. Clancy and N.F. Cramer, J. Plas. Phys. 35, 75 (1985).

I.J. Donnelly, B.E. Clancy and M.H. Brennan in 13th European Conf. on Controlled Fusion and Plasma Heating, Schliersee, Vol. 1, 431 (1986).

A.G. Elfimov in Proc. of the 2nd Joint Grenoble-Varenna Int. Symp. on Heating in Toroidal Plasmas, Como, Vol. 2, p. 683 (1980).

A. Hasegawa and L. Chen, Phys. Rev. Lett. 35, 370 (1975).

A. Hasegawa and L. Chen, Phys. Fluids 19, 1924 (1976).

B. Joye, A. Lietti. J.B. Lister, J.-M. Moret and W. Simm, Phys. Rev. Lett. 56, 2481 (1986).

A. Lietti and G. Besson, J. Phys. E. 19, 110 (1986).

D.W. Ross, G.L. Chen and S.M. Mahajan, Phys. Fluids 25, 652 (1982).

F. Yasseen and J. Vaclavik, Lausanne report, LRP 302/86 (1986).